Mantle transition zone topography and structure beneath the Yellowstone hotspot

David Fee and Ken Dueker

Department of Geology and Geophysics, University of Wyoming, Laramie, Wyoming, USA

Received 31 May 2004; revised 27 July 2004; accepted 9 August 2004; published 17 September 2004.

[1] The depths of the 410 and 660 km discontinuities beneath the Yellowstone hotspot are constrained using common conversion point imaging of P-wave receiver functions. The mean depth of the 410 and 660 is 411 ± 1.5 km and 656 ± 1.6 km, with 36–40 km of peak to peak topography. This topography is spatially uncorrelated, providing no evidence for a lower mantle plume currently beneath the hotspot. The topography suggests that ±200°C thermal anomalies exist with respect to an average mantle adiabat. Two warmer than normal regions are found: at the 410 to the NNW of the hotspot and at the 660 to the NE. Colder temperatures exist at the 410 under central Wyoming. Upper mantle convection and/or intermittent heat and mass transfer across the 660 may be responsible for the uncorrelated topography. Three negative arrivals about the 410 and 660 are observed that display correct P_ds moveout. *INDEX TERMS:* 7207 Seismology: Core and mantle; 7218 Seismology: Lithosphere and upper mantle; 8121 Tectonophysics: Dynamics, convection currents and mantle plumes; 8124 Tectonophysics: Earth's interior—composition and state (1212). **Citation:** Fee, D., and K. Dueker (2004), Mantle transition zone topography and structure beneath the Yellowstone hotspot, *Geophys. Res. Lett.*, *31*, L18603, doi:10.1029/2004GL020636.

1. Introduction

[2] Hypotheses for the dynamical origin of the Earth's hotspots can be divided into three categories: plumes rise from a thermal boundary layer at the base of the mantle; secondary intermediate scale convection develops in the upper mantle; or, hotspot magmatism derives from lateral variations in lithospheric thickness, fertility, and stress state [*Courtillot et al.*, 2003]. Evidence for a deep mantle plume driving the Yellowstone hotspot derives from the time-transgressive track of silicic volcanism approximately parallel to absolute plate motion and elevated $^3He/^4He$ ratios [*Armstrong et al.*, 1975]. Others suggest that some combination of active extension along the hotspot track, pre-existing lithospheric flaws, or edge driven convection are driving the hotspot [*Christiansen et al.*, 2002; *King and Anderson*, 1998]. Lastly, evidence for small-scale upper mantle convection beneath the western U.S. is provided by the observation of significant uncorrelated topography at the 410 and 660 discontinuities [*Dueker and Sheehan*, 1997; *Gilbert et al.*, 2003].

[3] Because these hotspot hypotheses make different predictions concerning the thermal structure of the mantle transition zone, a good test is to measure variations in the depth of the 410 and 660 km velocity discontinuities with P-S converted phases (P_ds) [*Gao et al.*, 2002; *Gilbert et al.*, 2003; *Lebedev et al.*, 2002]. The positive and negative Clapeyron slopes for the 410 and 660, respectively, predict that a vertically coherent transition zone thermal anomaly will move the 410 and 660 depths in an opposite (anti-correlated) direction [*Bina and Helffrich*, 1994]. This anti-correlation of discontinuity topography assumes that the seismic signals from these discontinuities are predominantly sampling the velocity discontinuities associated with the olivine phase loops and that thermal effects alone are modulating their depths [*Lebedev et al.*, 2002]. It may be that water content [*Smyth and Frost*, 2002], composition, and coupling between the garnet-pyroxene mineralogy [*Weidner and Wang*, 1998] may be creating topography, but our analysis cannot accurately constrain these effects.

2. Data and Methods

[4] Events with $M_b > 5.3$ and epicentral distances between 30–95° are selected from the Yellowstone, Billings, and SRP-93 PASSCAL deployments, and USNSN stations (Figure 1). Radial and tangential receiver functions (RF) are constructed using water level deconvolution

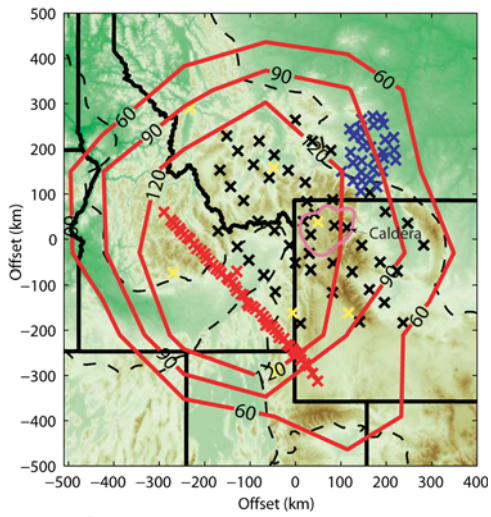

Figure 1. Stations locations and binned receiver function sampling density. Black x's denote YISA array, blue Billings, red SRP93, and yellow USNSN. Red contours indicate number of RF in 180 km square bins at 660 km depth. Dotted lines indicate tectonic provinces. Yellowstone caldera outlines the hotspot's current location.

0094-8276/04/2004GL020636$05.00

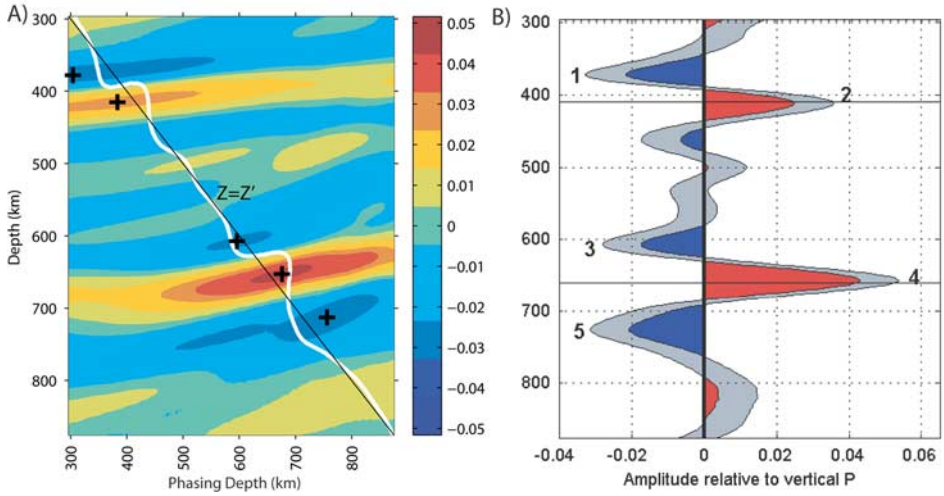

Figure 2. Phasing analysis and global stack. (a) Phasing diagram for all data. Positive arrivals with correct P_ds moveout occur at 410 and 660 km depth, while negative P_ds arrivals occur at 390, 610, and 720 km. $Z = Z'$ represents the line where the predicted P_ds arrival depth (phasing depth) equals the model depth. (b) Global stack of data from $Z = Z'$ in (a). Numbers denote P_ds arrivals: 1, '380'; 2, '410'; 3, '610'; 4, '660'; and 5, '720'. Gray shaded area indicates 95% confidence intervals. The arrival time of the 410 and 660 arrivals for a reference ray parameter of 6.4 s/deg is 45.6 and 69.5 s respectively.

[*Clayton and Wiggins*, 1976] and are then bandpass filtered between 20–7 s. An optimal water level for each deconvolution is chosen for the initial dataset of 7500 RF by using the 'corner' water level value in a resolution versus variance plot. Then 2500 RF are selected by requiring the standard deviation of the radial RF to be <0.75 of the mean standard deviation. P_ds moveout is removed using the flat layer P_ds moveout equations [*Vinnik*, 1977]. To map time to depth, an average 1-D surface wave S_v model derived from analysis of the stations in Figure 1 [*Schutt and Dueker*, in review] was used in the upper 200 km and smoothly merged with the AK135 radial P- and S-wave velocity model. The P-wave model above 200 km was specified to be the S_v model scaled by the V_p/V_s ratio of the AK135 model. The most remarkable feature of the average surface wave velocity model is a low velocity channel between 60–140 km depth with a minimum velocity of 4.0 km/sec at 80 km. We note that the sole effect of the use of this modified AK135 velocity model was to pull-up to depths of the mantle discontinuities by 6 km with respect to the unmodified AK135 velocity model. This velocity pull-up brought our estimates of the mean depths of the 410 and 660 to within one-sigma of the global mean depths. Corrections for lateral velocity heterogeneity in the upper 200 km are made by calculating relative P_ds timing corrections using the teleseismic P-wave residuals and the AK135 V_p/V_s ratio. Note this procedure only corrects for relative velocity heterogeneity above 200 km depth and the absolute depths are dependent upon the 1-D velocity model. Comparison of the stacks with and without the timing corrections shows the corrections slightly increase discontinuity amplitudes and create only minor changes in the topography.

[5] Common conversion point (CCP) stacking [*Dueker and Sheehan*, 1997] is performed using 180 km square by 2 km vertical bins The bin values are calculated at a horizontal grid spacing (pixel width) of 60 km, resulting in 67%, 33%, and 0% data sharing between points separated by 1, 2, and 3 pixels,. The bin size is comparable in size to the Fresnel zone of a 7 s P_{660}s phase and results in 50–160 RF per bin. To compare the effects of different bin sizes, the supplemental figure[1] presents a CCP image with 50% sharing between 120 km square by 2 km vertical bins. Absolute discontinuity depths are estimated to be accurate to 8 km, due to uncertainties in the V_p/V_s ratio in the upper 200 km [*Schutt and Humphreys*, 2004]. The accuracy of our average transition zone thickness is estimated to be ±4 km; this assumes that peak to peak bounds on transition zone velocity heterogeneity are ±2% V_{sv} [*Ritsema et al.*, 2004]. Discontinuity depths are estimated by finding the depth of the peak arrival about each discontinuity. Errors are estimated by taking spread estimates from depth distribution functions constructed from 200 bootstrapped realizations. This procedure finds that the 95% confidence bounds of the discontinuity depths are 1–3 km.

3. Results

[6] Because free-surface reverberations and coherent signal generated noise may create false arrivals that could be misinterpreted as P_ds arrivals, phasing analysis is performed to identify which arrivals display correct P_ds moveout (Figure 2) [*Vinnik*, 1977]. Phasing analysis of the entire RF dataset shows that in addition to the 410 and 660 km discontinuities, negative arrivals from 380, 620, and 700 km display correct P_ds moveout. In addition, when the dataset is split into 4 geographic quadrants, the 410 and 660 phase correctly while the negative arrivals phase correctly in the NW and SW geographic quadrants. A global stack of all the RF reveals mean depths of 411 ± 1.5 km and 656 ± 1.6 km for the 410 and 660 (Figure 2), within the errors of global estimates [*Flanagan and Shearer*, 1998]. Our mean transition zone thickness is 245 km, within the error of the 242 km global average.

[7] Inspection of the CCP image reveals the edges of the image volume have larger amplitudes due to the loss of

[1] Auxiliary material is available at ftp://ftp.agu.org/apend/gl/2004GL020636.

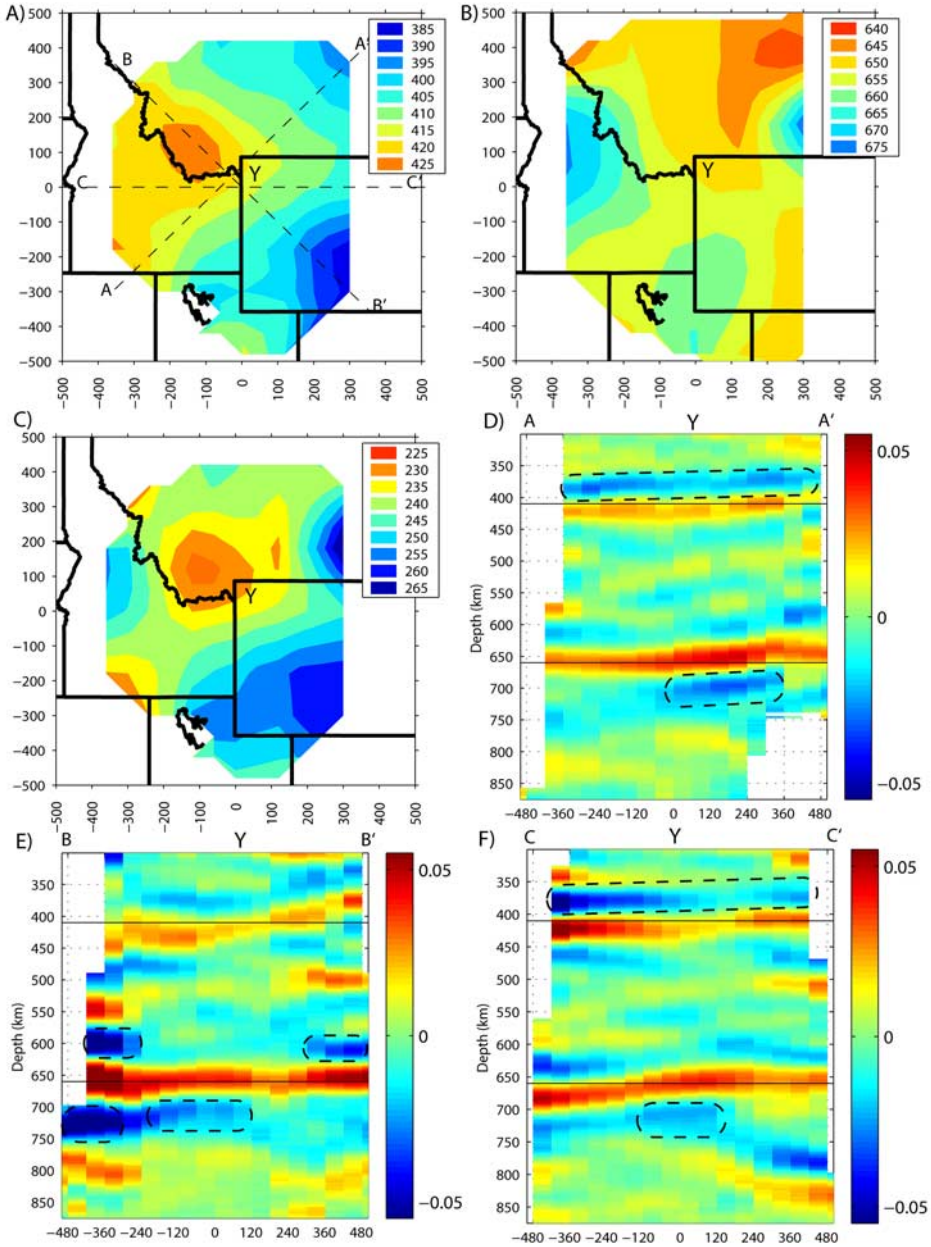

Figure 3. Non-interpolated CCP images. The only lateral smoothing imposed by our processing is a three pixel correlation associated with bin sharing discussed in the text. Y symbol denotes Yellowstone hotspot location. (a) 410 discontinuity topography. (b) 660 discontinuity topography. (c) Transition zone thickness. (d),(e),(f) Cross sections through CCP image labeled in (a).

data-fold and hence ray parameter distribution (Figure 3). The 410 discontinuity has 40 km of peak to peak topography, with a deep 410 (428 km) to the NNW of the hotspot location (Dillon, MT anomaly) indicating warmer than normal temperatures. The Dillon anomaly is chiefly responsible for thinning the transition zone in this region to 224 km, as the 660 is relatively flat. Similarly, a shallow 410 near Green River, Wyoming (Green River anomaly) is primarily responsible for thickening the transition zone in this region to 265 km, as the 660 is relatively flat. The 660 has 36 km of topography, with most of the topography along the east and west edges of the image volume. Topography between the 410 and 660 discontinuities is not correlated.

[8] Figure 2 shows three negative polarity arrivals from 380, 610, and 720 km depth that phase correctly as $P_d s$ arrivals. However, because these arrivals are adjacent to the 410 and 660 arrivals, the magnitude of the negative sidelobes associated with our filtered RF must be considered. The amplitude of the filtered vertical component RF sidelobe is 20% with respect to the P-wave arrival. Thus, the 410/380 discontinuity amplitude ratio of one and the lack of a negative "arrival" below the 410 argues that the 380 is not a sidelobe artifact. Also, the CCP image shows the 380 arrival is laterally continuous across the image volume in cross-section A-A′ and C-C′. In contrast, the two negative arrivals above and below the 660 have an amplitude half that of the 660 arrival. The 720 is robustly imaged within

the middle of the CCP image volume below the Yellowstone hotspot, while the 610 arrival occurs mainly along the edges (Figure 3).

4. Discussion

[9] Although significant transition zone topography indicates a thermally heterogeneous transition zone, no throughgoing plume conduit is found. The Dillon anomaly suggests a 200° temperature increase to the west of the hotspot, and preliminary correlation with a Yellowstone P-wave tomographic model [*Yuan and Dueker*, in review] indicates a correlation with a low-velocity pipe extending from the hotspot to the 410 Dillon anomaly. However, predicted temperatures at the 660 are near normal below the Dillon anomaly. This suggests that this warm 410 anomaly does not extend across the 660. Uncorrelated 410 and 660 topography is not an uncommon observation in the western US. A dynamical model to explain this observation is that convective cells confined to the upper mantle are dominating the 410 thermal structure [*Gilbert et al.*, 2003]. If a lower mantle origin for the hotspot is preferred, then intermittent heat and mass transfer across the 660 [*Yuen et al.*, 1998] could explain our discontinuity topography observations.

[10] To our knowledge, the finding of a 720 km negative velocity contrast arrival is the first time it has been reported. This could be due to the relatively high-fold of the dataset or this discontinuity may be unique to the dynamics of this region. The 380 negative discontinuity has been proposed to manifest the release of water (causing wet melting) from mantle flux across the 410 [*Bercovici and Karato*, 2003]. More detailed analysis of these arrivals is presented in Dueker et al. [in review] with the higher data-fold Billings array (Figure 1).

[11] **Acknowledgment.** We thank the NSF Continental Dynamics Program for funding this research and the PASSCAL instrument center.

References

Armstrong, F. C., W. P. Leeman, and H. E. Malde (1975), K-Ar dating, Quaternary and Neogene volcanic rocks of the Snake River Plain, Idaho, *Am. J. Sci.*, *275*, 225–251.

Bercovici, D., and S. I. Karato (2003), Whole-mantle convection and the transition-zone water filter, *Nature*, *425*, 39–44.

Bina, C. R., and G. Helffrich (1994), Phase transition Clapeyron slopes and transition zone seismic discontinuity topography, *J. Geophys. Res.*, *99*, 15,853–15,860.

Christiansen, R. L., G. R. Foulger, and J. R. Evans (2002), Upper-mantle origin of the Yellowstone hotspot, *Bull. Geol. Soc. Am.*, *114*, 1245–1256.

Clayton, R. W., and R. A. Wiggins (1976), Source shape estimation and deconvolution of teleseismic body waves, *Geophys. J. R. Astron. Soc.*, *47*, 151–177.

Courtillot, V., A. Davaille, J. Besse, and J. Stock (2003), Three distinct types of hotspots in the Earth's mantle, *Earth Planetary Sci. Lett.*, *205*, 295–308.

Dueker, K. G., and A. F. Sheehan (1997), Mantle discontinuity structure from midpoint stacks of converted P and S waves across the Yellowstone hotspot track, *J. Geophys. Res.*, *102*, 8313–8327.

Flanagan, M. P., and P. M. Shearer (1998), Global mapping of topography on transition zone velocity discontinuities by stacking SS precursors, *J. Geophys. Res.*, *103*, 2673–2692.

Gao, S. S., P. G. Silver, K. H. Liu, and Kaapvaal Seismic Group (2002), Mantle discontinuities beneath Southern Africa, *Geophys. Res. Lett.*, *29*(10), 1491, doi:10.1029/2001GL013834.

Gilbert, H. J., A. F. Sheehan, K. G. Dueker, and P. Molnar (2003), Receiver functions in the western United States, with implications for upper mantle structure and dynamics, *J. Geophys. Res.*, *108*(B5), 2229, doi:10.1029/2001JB001194.

King, S. D., and D. L. Anderson (1998), Edge-driven convection, *Earth Planet. Sci. Lett.*, *160*, 289–296.

Lebedev, S., S. Chevrot, and R. D. van der Hilst (2002), Seismic evidence for olivine phase changes at the 410- and 660-kilometer discontinuities, *Science*, *296*, 1300–1302.

Ritsema, J., H. J. van Heijst, and J. H. Woodhouse (2004), Global transition zone tomography, *J. Geophys. Res.*, *109*, B02302, doi:10.1029/2003JB002610.

Schutt, D. L., and E. D. Humphreys (2004), *P* and *S* wave velocity and V_P/V_S in the wake of the Yellowstone hot spot, *J. Geophys. Res.*, *109*, B01305, doi:10.1029/2003JB002442.

Smyth, J. R., and D. J. Frost (2002), The effect of water on the 410-km discontinuity: An experimental study, *Geophys. Res. Lett.*, *29*(10), 1485, doi:10.1029/2001GL014418.

Vinnik, L. P. (1977), Detection of waves converted from P to SV in the mantle, *Phys. Earth Planet. Inter.*, *15*, 39–45.

Weidner, D. J., and Y. Wang (1998), Chemical- and Clapeyron-induced buoyancy at the 660 km discontinuity, *J. Geophys. Res.*, *103*, 7431–7441.

Yuen, D. A., L. Cserepes, and B. A. Schroeder (1998), Mesoscale structures in the transition zone: Dynamical consequences of boundary layer activities, *Earth Planets Space*, *50*, 1035–1045.

K. Dueker and D. Fee, Department of Geology and Geophysics, University of Wyoming, 1000 University Avenue, Laramie, WY 82070, USA. (fee@uwyo.edu)